Contents lists available at ScienceDirect

Applied Catalysis B: Environmental

The synergistic effects of Ru and WO_x for aqueous-phase hydrogenation of glucose to lower diols

Yi Liu, Yuliu Liu, Yi Zhang[*]

State Key Laboratory of Organic-Inorganic Composites, Department of Chemical Engineering, Beijing University of Chemical Technology, Beijing, 100029, China

ARTICLE INFO

ABSTRACT

Aqueous-phase hydrogenation of glucose to lower diols (ethylene glycol (EG), 1, 2-propylene glycol (PG), and butanediol (BDO)) over bi-functional Ru-W supported catalysts was investigated in a continuous-flow fixed-bed reactor. A variety of catalysts based on different supports including mesoporous SiO_2, activated carbon (AC), carbon nanofibers (CNFs), and bulk WO_3 were compared and examined by N_2 physisorption, H_2 chemisorption, XRD, TEM, ICP, H_2-TPR, *in-situ/ex-situ* XPS, NH_3-TPD, and Raman spectra. The results indicate that the lower diols yield is highly dependent on the synergistic effect of Ru metal sites and WO_x acid sites, in other words, strongly depending on the competitive reactions of the glucose. Abundant W^{4+} and Ru° sites on Ru-W/SiO_2 catalysts with large specific surface area effectively catalyze the selective cleavage of the C−C bonds in glucose and subsequent hydrogenation to lower diols, resulting in 100% glucose conversion as well as highest diols selectivity (87.3%) over 50 h reaction at 478 K and 4 MPa H_2. Meanwhile, the Ru/WO_3 with much lower surface area forms more W^{5+} species, which is advantageous to producing more EG products (55.9%) at the same reaction conditions.

1. Introduction

Strict emission legislation for the combustion of fuels requires the development of clean technologies, minimizing the environmental impact. Carbohydrates, represent 75% of the annual renewable biomass, are an attractive source of biogenic carbon from which sustainable fuels and various value-added chemicals can be derived [1,2]. Among various carbohydrates, cellulose is the most abundant source of biomass and has received considerable attention as a vitally renewable alternative to fossil fuels [3]. Glucose, which can be obtained from the depolymerization of cellulose by catalysis of liquid mineral acids or solid acids, is an ideal feedstock in future large-scale biorefining due to the simply molecular structure, energy saving and environmentally friendly reaction process [4]. In past several decades, conversion of cellulose or glucose into various chemicals, such as various alcohols [5–8], fuels or fuel additives [9], lactic acid [10,11], formic acid (FA) [12], 5-hydroxymethylfurfural (HMF) [13–15], γ-Valerolactone (GVL) [16], has been studied extensively. Among them, one of the most promising processes for biomass transformation is the catalytic hydrogenolysis of biomass to polyols; especially lower diols, such as ethylene glycol (EG), 1, 2-propylene glycol (PG), and butanediol (BDO), which are important raw materials for antifreeze, drug intermediates, polyester resins, cosmetics, etc [4,17].

Hydrogenation of cellulose or glucose to corresponding polyols (such as sorbitol and mannitol) in industrial processes can be performed over Raney-type nickel catalysts [18]. However, the drawback of Ni catalysts is the leaching of nickel and associated metal sintering those results not only in the on-stream deactivation but also in the increased purification costs since product contamination by nickel. These drawbacks can be overcome by using a different hydrogenation catalyst, for instance ruthenium catalysts. In 2006, Fukuoka et al. [19] reported that Ru catalysts supported on inorganic oxides had high activity for the conversion of cellulose into sugar alcohols in water under hydrogen pressure. They found that the Ru/oxide worked as a bi-functional catalyst for the hydrolysis of cellulose and subsequent reduction to sugar alcohols with the highest yield of 31%. Liu et al. [20] reported a green approach to efficient conversion of cellulose into hexitols together with other lighter polyols used supported Ru/C catalyst in hot water, which provided the yield of hexitol of up to 39.3% after 30 min in 6 MPa H_2 at 518 K.

However, if the target product are changed from polyols to lower diols, the reaction route becomes complex. After hydrolysis of cellulose in the presence of strong mineral acids (e.g., H_2SO_4, H_2WO_4), glucose or fructose not only undergo retro-aldol condensation (RAC) reaction to form C_2-C_4 intermediates (glycolaldehyde, erythrose and dihydroxyacetone), but also can be directly hydrogenated into polyols, which are

* Corresponding author.
  E-mail address: yizhang@mail.buct.edu.cn (Y. Zhang).

inert for RAC reactions and difficult to further degrade into C_2-C_4 small molecules for lower diols formation [17,21]. Hence, preferentially break the C−C bonds in C_6 sugars to form C_2-C_4 intermediates before the directly hydrogenation of C_6 sugars is very critical.

A breakthrough in the catalytic conversion of cellulose to lower diols was first reported by Zhang and Chen et al. in 2008 [22]. They observed that W-based catalysts promoted by a small amount of nickel can effectively catalyze cellulose conversion into polyols, especially ethylene glycol (EG) and sorbitol in batch experiments. After that, extensive studies were conducted by many researchers worldwide to explore new catalysts to tuning the reaction performance. Recently, Liu et al. [21] found that WO_3 promoted Ru/C catalysts enable efficient conversion of cellulose into ethylene glycol (51.5%) and propylene glycol (6.7%) with cellulose conversion of 23.4% after 30 min at 478 K and 6 MPa H_2. They found that the catalytic process and the yield of polyols were influenced by supports and surface density/dispersion of WO_3 species. Wang et al. [23] compared the nickel-based catalysts with various supports in the batchwise hydrogenolysis of cellulose to 1, 2-alkanediols, and found that the choice of supports plays a critical role in the product distribution and selectivity. The best result was obtained by using ZnO as the support, with complete cellulose conversion and remarkable lower diols yield of 70.4% after 2 h at 518 K.

In the present work, we report an efficient and stable conversion of glucose to lower diols, including EG, 1, 2-PG, and 1, 2-BDO, as dominant products in the continuous-flow fixed bed reactor via supported Ru-W catalysts. The advantages of the continuous-flow fixed bed process are narrow products distribution, the higher space-time yield and the absence of the expensive separation of the catalyst. Ru-W catalysts over different supports (SiO_2, CNFs, AC, and WO_3) were synthesized and evaluated to investigate the synergistic effects of Ru and WO_x on the catalyst performance for glucose hydrogenation. All obtained catalysts were characterized by N_2 physisorption, H_2 chemisorption, XRD, TEM, ICP, H_2-TPR, *in-situ/ex-situ* XPS, NH_3-TPD, and Raman spectra.

2. Experimental

2.1. Catalyst preparation of supported Ru-W catalysts

The Ru-W/SiO_2 catalyst was prepared by a stepwise incipient wetness impregnation method on commercially available silica gel (pore volume 1.061 ml/g, pore diameter 6.7 nm, BET = 451.2 m^2/g). The loading of Ru and W were 1 wt. % and 10 wt. %, respectively. First, the aqueous solution of ammonium metatungstate hydrate $((NH_4)_6H_2W_{12}O_{40} \cdot xH_2O$, Sigma-Aldrich Co.) was impregnated onto silica support followed by drying at 393 K for 12 h under ambient conditions. After that, the sample was calcinated at 673 K for 2 h. Second, this calcined sample was impregnated again with an aqueous solution of ruthenium (III) chloride (Sigma-Aldrich Co.). Afterwards, the sample was again dried at 393 K for 12 h, then by calcinations at 673 K for 2 h.

In a similar procedure, Ru-W/AC catalyst was prepared using activated carbon (AC, Sigma-Aldrich Co.) as support. The differences are that the AC supports were treated with nitric acid solution (33 wt. %) at 353 K for 24 h in order to increase the hydrophilicity by introducing surface carboxylic groups. And the catalyst precursor was calcined in the atmosphere of nitrogen. The Ru-W/CNFs catalysts were prepared with the similar procedure as Ru-W/AC, except that the CNFs (Aldrich) supports were treated with nitric acid solution (66 wt. %) at 353 K for 8 h prior to the deposition of active metal component. The loading of Ru and W were 1 wt. % and 10 wt. %, respectively. The Ru/WO_3 catalyst was prepared by overloading impregnation of aqueous solutions of ruthenium (III) chloride on tungsten oxide (WO_3) supports (Aladdin Co.). The loading of Ru was 1 wt. %. The preparation procedure was as described for the Ru-W/SiO_2 catalysts. All samples were pressed into pellets (10 MPa), crushed and sieved to retain 20–40 mesh particles for reaction tests.

2.2. Catalyst characterization

Powder X-ray diffraction (XRD) patterns of the passivated and used catalysts were recorded on XRD-6000 (Shimadzu, Japan) using Cu Kα radiation (λ = 0.154 nm) at 40 kV and 30 mA. HR-TEM measurements were performed on a FEI Tecnai G2 F20 S-Twin transmission electron microscope at an acceleration voltage of 200 kV.

NH_3 temperature-programmed desorption (NH_3-TPD) measurements were conducted on Quantachrome autosorb iQ equipment (Quantachrome, USA). The Brunauer-Emmett-Teller (BET) surface area was calculated based on N_2 adsorption-desorption data obtained by Micromeritics ASAP 2020 equipment (Micromeritics, USA). Ru dispersions were measured by H_2-O_2 titration using an ASAP 2020 Micromeritics apparatus with the procedures reported in literature [24].

Raman spectra were recorded at room temperature with Renishaw inVia (UK) spectrometer using the 532 nm argon ion laser. ICP experiments were carried out on a Thermo IRIS Intrepid II atomic emission spectrometer to test the actual metal loading of catalysts as prepared and after reaction.

H_2-Temperature programmed reduction (H_2-TPR) experiments were carried out in a quartz tube reactor using 0.05 g calcined catalysts. The reducing gas, a mixture of 10% H_2 diluted by Ar, was fed via a mass flow controller at 30 ml/min and the temperature was increased from 300 K until 1100 K at a rate of 8 K/min. The effluent of reactor passed through a 5 Å molecular sieve trap to remove produced water, before reaching TCD.

In-situ XPS experiments were performed at the photoemission end-station at beamline BL10B in the National Synchrotron Radiation Laboratory (NSRL) in Hefei, China. The beamline is connected to a bending magnet and covers photon energies from 60 to 1000 eV with a resolving power (E/ΔE) better than 1000. The end-station is composed of four chambers, i.e., analysis chamber, preparation chamber, quick sample load-lock chamber and high pressure reactor. The analysis chamber, with a base pressure of < 2 × 10^{-10} torr, is connected to the beamline and equipped with a VG Scienta R3000 electron energy analyzer and a twin anode X-ray source. The high pressure reactor houses a reaction cell where the samples can be treated with different gases up to 20 bar and simultaneously heated up to 923 K. After the sample treatment, the reactor can be pumped down to high vacuum (< 10^{-8} torr) for sample transfer. In the current work, the pre-reduced samples were pressed into thin pellets and then placed into the reaction cell and reduced in a flowing H_2 under atmospheric pressure at 648 K for 2 h. Then the samples were cooled down to room temperature and transferred to the analysis chamber under vacuum conditions for measurements.

Ex-situ X-ray photoelectron spectroscopy (XPS) measurements were collected on VG Scientific ESCALAB 250 spectrometer with the monochromatized Al Kα source (1486.6 eV).

2.3. Catalyst evaluation tests

Hydrogenation of glucose was carried out in a continuous-flow fixed-bed stainless steel reactor (8 mm I.D.) at 478 K, 4 MPa H_2 and GHSV (H_2) = 2500 cm^3 g^{-1} h^{-1}. The glucose aqueous solution (5 wt. %) was introduced to flowing gas streams using a liquid infusion pump (LC-20AT, Shimadzu) with a flow rate of 0.5 ml/min. Exhaust transfer lines were kept at 423 K to ensure that no condensation of liquid reactants or products occurred in front of the cold trap. About 0.5 g catalysts (20–40 mesh) was packed in the middle of reactor which was heated in a muffle furnace. The reaction temperature of catalyst bed was monitored by a K-type thermocouple controlled by a PID controller. Prior to reaction, the catalysts were reduced by pure H_2 for 10 h at atmospheric pressure, 648 K and GHSV (H_2) = 9000 cm^3 g^{-1} h^{-1}. The effluent gas was on-line analyzed by gas chromatograph (GC-2014C, Shimadzu) equipped with a thermal conductivity detector
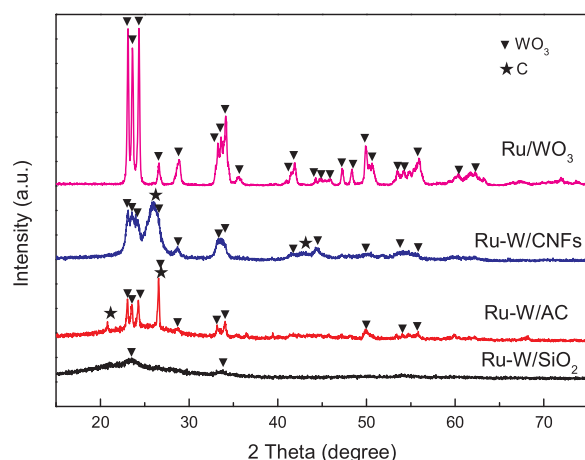
Fig. 1. XRD patterns of various Ru-W supported catalysts as prepared.

(TCD). The liquid-phase products composition was off-line analyzed every 5 h by high-performance liquid chromatography (HPLC) (Waters 2414, RI detector) equipped with a shodex SH-1011 column (7 μm, 8 x 300 mm). The mobile phase was 5 mM H_2SO_4 with a flow rate of 0.5 ml/min. The temperature of the column and detector was 50 °C and 40 °C, respectively.

3. Results and discussion

3.1. Catalysts characterization

3.1.1. Structural properties of Ru-W supported catalysts

To evaluate the phase changes of tungsten and ruthenium species during the reaction process, we performed XRD examinations on both fresh and used catalysts (Figs. 1 and 2). The XRD patterns of fresh catalysts are shown in Fig. 1. No diffraction peaks of Ru species were observed for all catalysts, indicating the formation of highly dispersed Ru species due to the low loading (1 wt. %). The Ru-W/SiO_2 sample exhibit a broad diffraction peak in the 2θ range between 10° and 30°, which can be ascribed to the amorphous SiO_2 [25]. The diffractogram of Ru/WO_3, Ru-W/CNFs, and Ru-W/AC catalysts all show peaks associated with crystalline WO_3 phase (JCPDS 20–1324), while these peaks were hardly observed for Ru-W/SiO_2 catalyst. This result suggests that the highly dispersed WO_3 species were obtained in Ru-W/SiO_2 catalyst due to the rich OH group of the silica surface [26] and large BET surface area, which would realize more active tungsten oxide sites in this reaction. Meanwhile, the highest intensity of WO_3 characteristic peaks for
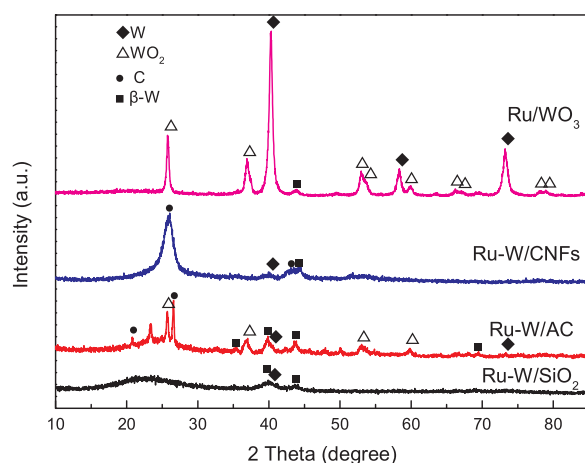

Fig. 2. XRD patterns of various Ru-W supported catalysts after reaction at 478 K for 10 h.

the Ru/WO_3 catalyst can be ascribed to contribution of bulk WO_3 support. The crystallite sizes of WO_3 were calculated with the Scherrer equation using the parameters obtained by XRD, as compared in Table 1.

The XRD patterns of the used Ru-W supported catalysts after reaction are displayed in Fig. 2. It can be found that the peaks assigned to WO_3 phase were disappeared in all catalysts compared with that of the fresh samples, while XRD peaks associated with W (JCPDS 04-0806) and β-W (JCPDS 47–1319) were observed for all samples. β-W, which contains a small amount of oxygen, is a metastable form of α-W that can decompose into W and WO_2 [27]. Furthermore, Ru/WO_3 and Ru-W/AC catalysts exhibit dominant diffraction peaks of typical crystalline WO_2 (JCPDS 32–1393) at 25.7°, 37.0°, and 53.1°. These results indicate that the reduction of WO_3 to W or WO_2 was continuously proceeding during the reduction and reaction process. Regarding Ru-W/CNFs catalyst, the tungsten species must have experienced serious leaching during reaction due to the non-porous structure of CNF and the weak metal-support interaction, which results in the peak intensity of tungsten crystal phase decreased dramatically after reaction compared with fresh sample. This hypothesis was further confirmed by ICP results (Table 1).

Fig. 3 shows HR-TEM images of all used Ru-W supported catalysts after glucose hydrogenolysis reaction. The images indicate that large (20–40 nm) WO_2 particles are formed for Ru/WO_3 bulk catalyst, while small particles with sizes less than 5 nm are highly dispersed on the AC, CNFs and silica support. It is well know that the support with a larger BET surface area (AC and SiO_2) favors the dispersion of metal particles, and leads to the formation of strong metal-support interaction, which would suppress the reduction of WO_3. As shown in Fig. 3c–d, for used Ru-W/AC and Ru-W/SiO_2 catalysts, the lattice distances of 0.345 nm and 0.385 nm could be attributed to the (011) and (001) planes of WO_2 and WO_3, respectively. However, the Ru-W/CNFs catalyst also exhibited remarkable small particle size (< 5 nm) and distributed homogeneously (Fig. 3b). This is probably due to the significant leaching of large tungsten particles with weak metal-support interaction, which leads to the presence of residual small W° particles on the CNFs support. This implies that the reduction of tungsten trioxide to WO_2 or W species in Ru-W/AC and Ru-W/SiO_2 catalysts was difficult compared with the Ru-W/CNFs sample, due to the stronger metal-support interaction between the smaller crystalline size of WO_3 and support. This conclusion is in good agreement with the XRD data.

In order to further explore the reduction behavior of the Ru-W supported catalyst, the H_2 temperature programmed reduction (H_2-TPR) results were discussed. The pure SiO_2, bulk WO_3, Ru/SiO_2, and W/SiO_2 were used as reference samples to distinguish the reduction peaks of various phase. As shown in Fig. 4, the Ru/WO_3 catalyst which use bulk WO_3 as support shows three district H_2 consumption peaks with different areas between 400 K and 1000 K. According to literature data and reference samples, the first sharp peak at 450 K can be attributed to the reduction of ruthenium species, and the broad peak around 968 K and above 1000 K suggests the existence of reduction process of WO_3, i.e., $WO_3 \rightarrow WO_x \rightarrow W$ [28]. Furthermore, it displays a H_2 consumption peak at 675 K, which should be ascribed to the reduction of part of WO_3 strongly interacted with Ru. The comparison between WO_3 and Ru/WO_3 samples clearly shows that ruthenium promotes WO_3 to be reduced due to the role of the hydrogen spillover [29], resulting in the shift of reduction peaks to the lower temperature. It is generally known that dissociation of hydrogen takes place easily on the noble metal sites and the dissociated hydrogen can spill-over to the oxide support. Because such spill-over hydrogen is quite active, the reduction of the oxide can proceed easy than that for the pure oxide [30]. This promotion effect by Ru was also observed in Ru-W/SiO_2, Ru-W/CNFs, and Ru-W/AC catalysts. It should be noted that no obvious reduction peak of Ru species was found in Ru-W/CNFs and Ru-W/AC catalysts, this could be due to the different calcination atmosphere (N_2) in the preparation of carbon materials supported catalysts, which should prevent the oxidation of Ru° species. Moreover, in the case of Ru-W/

Table 1
The properties of various samples as prepared, after reduction and after reaction.

Catalysts	Ru actual loading (%)		W actual loading (%)		BET surface area (m^2/g)	Ru dispersion[c] (%)	WO_3 particle size (nm)		Amount of desorbed NH_3 ($\mu mol/g$)[f]	Contribution of $W4f_{7/2}$ (%)[g]		
	Fresh[a]	Used[b]	Fresh[a]	Used[b]			XRD[d]	TEM[e]		W^{6+}	W^{4+}	$W°$
Ru/WO$_3$	0.90	0.68	–	–	4.5	14.1	38.6	28.5	13.1	–	82.0[h]	18.0
Ru-W/SiO$_2$	1.02	1.00	10.1	9.8	406.2	43.2	–	4.6	150.1	62.3	16.1	21.6
Ru-W/CNFs	0.90	0.61	7.3	3.1	81.3	9.4	13.4	10.1	N.A.	–	–	–
Ru-W/AC	0.97	0.91	9.8	9.0	273.8	31.7	10.8	7.3	91.3	–	–	–

[a] Metal loading as determined by ICP analyses of fresh samples.
[b] Metal loading as determined by ICP analyses of used samples after reaction for 10 h.
[c] Determined by a H2-O2 titration technique.
[d] WO3 crystallite size as determined by X-ray diffraction of fresh samples.
[e] WO3 crystallite size as determined by TEM of fresh samples.
[f] The total acidity was determined by quantifying the desorbed NH3 below 850 K by NH3-TPD of reduced samples.
[g] Surface composition of W species in Ru-W/SiO2 catalyst as determined by in-situ XPS.
[h] Contribution of W4f7/2 from W5+.

SiO$_2$ and Ru-W/AC, the shifting of the reduction peak of WO$_3$ to a higher temperature compared with that of Ru-W/CNFs and Ru/WO$_3$ can be ascribed to the difficulty in reducing WO$_3$, which strongly interact with the support due to the smaller metal oxide crystalline size. This result is consistent with XRD and TEM.

Raman spectroscopy is used to determine the molecular structures of various Ru-W supported catalysts. As shown in Fig. 5, three Raman bands at about 806, 712, and 274 cm^{-1} appeared for all fresh and reduced catalysts except Ru-W/SiO$_2$, which could be assigned to W−O stretching, W−O bending, and W−O−W deformation modes in crystalline WO$_3$ nanoparticles, respectively [31]. For Ru-W/SiO$_2$ catalyst, the Raman spectra exhibited in a typical amorphous state, since no significant peaks appeared. The absence of Raman peaks related to tungsten species is probably due to the relatively low WO$_3$ loading (10 wt. %) and high specific surface area (451.2 m^2/g) of SiO$_2$, which leads to the formation of well dispersed WO$_3$ species on the surface of silica [32], as confirmed by XRD. This phenomenon was also observed by other researchers. Lu et al. [32] prepared a series of WO$_3$/SiO$_2$ catalysts with different WO$_3$ loading from 5 wt. % to 40 wt. % for selective oxidation of cyclopentene, and found that the Raman bands of tungsten oxide species was only observed when the loading of WO$_3$ is higher than 20 wt. %.

For the reduced catalysts, the Raman bands corresponding to tungsten oxide were considerably more diffuse than in the case of fresh samples, and some peaks were not even visible. Moreover, the most intensive three Raman bands all shift to lower energies, indicating the different oxidation states of the samples. It was reported that the chemical bonds of W^{6+} were stronger than those of reduced tungsten atoms [33,34]; thus, Raman peaks of W^{6+} bonds appeared at higher energies, i.e., higher wave numbers. Hence, the lower wave numbers of Raman bands for reduced catalysts indicate the reduction of WO$_3$ species to WO$_x$ under reduction conditions, which is in good coincidence with the results as indicated by H$_2$-TPR.

3.1.2. Acid properties of reduced Ru-W supported catalysts

Surface acidic properties of various Ru-W supported catalysts after reduced were compared by temperature-programmed desorption in an ammonia environment. As shown in Fig. 6, no noticeable TPD peak was found for Ru/WO$_3$ and Ru-W/CNFs catalysts due to the low support BET surface area and large tungsten particles. In contrast, the Ru-W/SiO$_2$ and Ru-W/AC catalysts both exhibit a broad peak where the maximum peak is located at ∼590 K and ∼740 K, respectively. This is
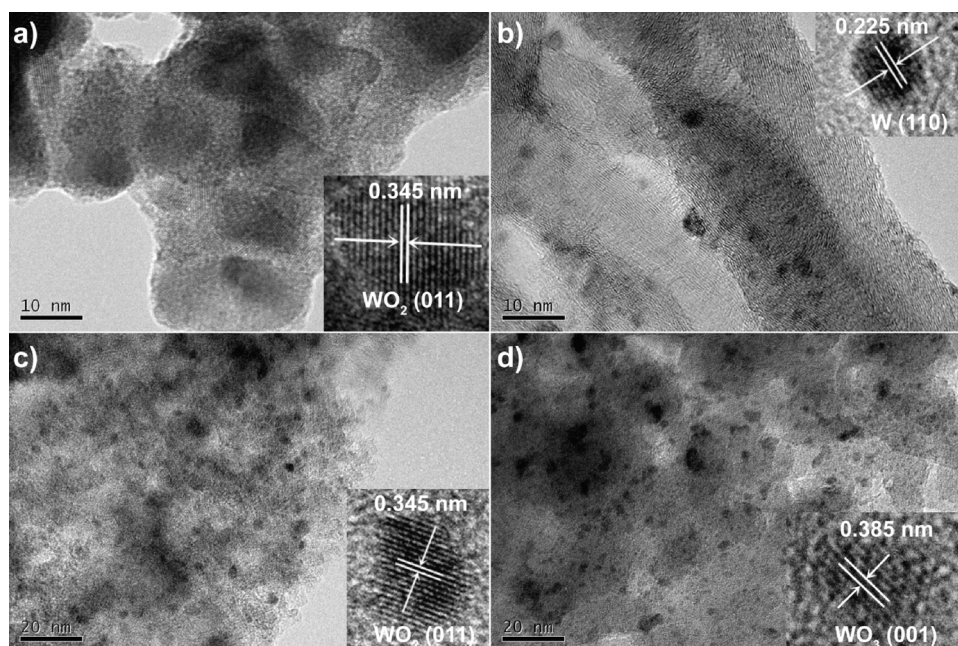

Fig. 3. HR-TEM images of all used Ru-W supported catalysts after reaction at 478 K for 10 h: (a) Ru/WO$_3$; (b) Ru-W/CNFs; (c) Ru-W/AC; (d) Ru-W/SiO$_2$.
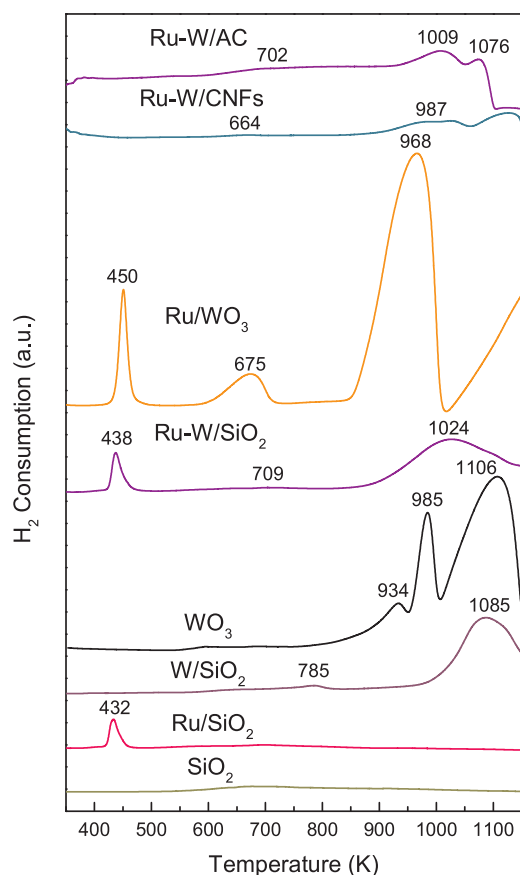
Fig. 4. H$_2$-TPR spectra of various Ru-W supported catalysts.

Fig. 6. NH$_3$-TPD spectra of various Ru-W supported catalysts reduced in H$_2$ at 648 K for 10 h.

contribute to enhance the selectivity of diols.

3.2. Effect of the support type on the catalytic performance in glucose hydrogenolysis

Table 2 summarizes the catalytic performances of various Ru-W catalysts with different support in glucose hydrogenolysis at 478 K, 4 MPa H$_2$ and GHSV (H$_2$) = 2500 cm^3 g^{-1} h^{-1}. For all reactions, diols (EG, 1, 2-PG, 1, 2-BDO) are the major products and very small amount of CH$_4$ was measured as an additional product. In addition, a wide variety of byproducts, including sorbitol, erythritol, glycerol, and 5-HMF were detected partly in some catalysts. Among the catalysts investigated, the Ru-W/SiO$_2$ catalyst were observably more effective and selective in producing lower diols, giving markedly higher selectivity and conversion compared with other catalysts in this work. Glucose conversion reached 100%, and the selectivities of EG, 1, 2-PG, and 1, 2-BDO were 33.8%, 29.2%, and 24.3%, respectively. The total selectivity to lower diols remained > 87% with time on stream. In contrast, the performance of Ru-W/AC was comparable to that of Ru-W/SiO$_2$, with 99.3% conversion of glucose and slightly lower total diol selectivity of 80.2%. However, in the case of Ru-W/CNFs sample, the product selectivity is dramatically changed. The selectivity of diols decreased to 44.7%, while sorbitol and glycerol were the predominant products with the selectivity of 36.8% and 14.7%, respectively. It is generally known that the hydrogenation of glucose to sorbitol can easily occur under mild conditions over metal sites such as Ni or Ru [4], and no acid sites

quite reasonable because the catalyst with smaller tungsten particles can have a larger amount of surface acid sites as long as the same amount of tungsten is loaded [27]. Furthermore, the peak at lower temperature for Ru-W/SiO$_2$ catalyst after reduced can be assigned to the desorption peak of ammonia adsorbed on the weak acid sites, while the high-temperature desorption peak for Ru-W/AC catalyst after reduced is the strong acid sites [35]. The calculated amount of acidity is listed in Table 1, and it can be arranged in the following order: Ru-W/SiO$_2$ > Ru-W/AC > Ru/WO$_3$ > Ru-W/CNFs. In the hydrogenolysis of glucose to diols, WO$_x$ crystallites plays a key role in generating solid acid sites to catalytically cleave the C−C bonds in the sugar molecules [21,36]. Hence, it is proposed that the abundant acid sites and moderate acid strength for Ru-W/SiO$_2$ catalyst in the present work would
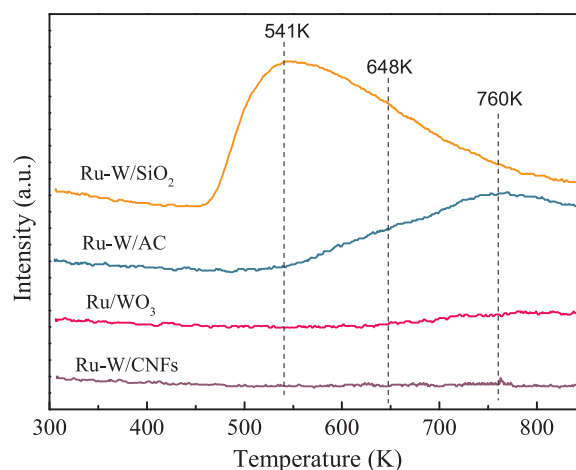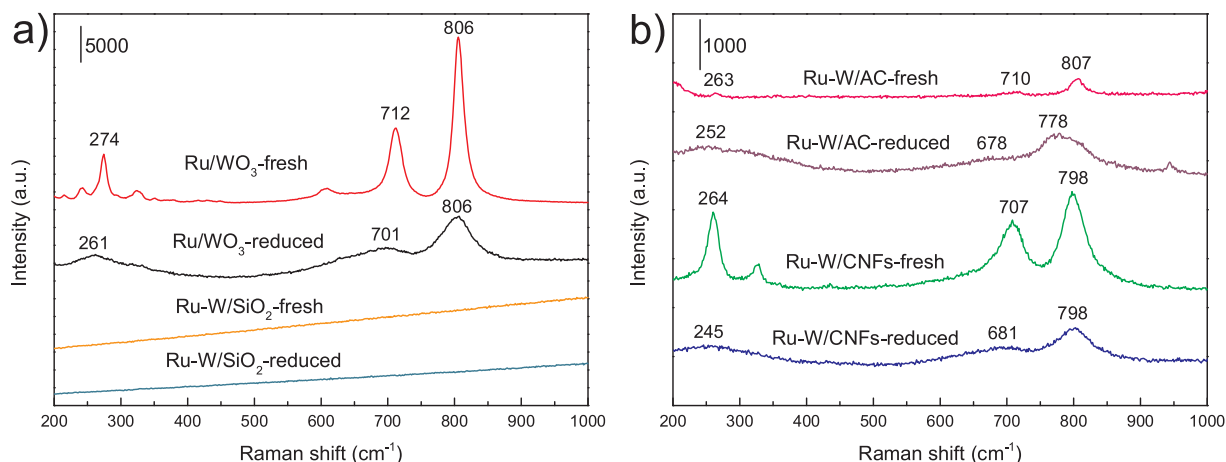

Fig. 5. Raman spectra of fresh and reduced Ru-W supported catalysts: (a) Ru-W/SiO$_2$ and Ru/WO$_3$; (b) Ru-W/CNFs and Ru-W/AC.

Table 2

Glucose conversion and diols selectivities of various Ru-W supported catalysts in fixed-bed reactor[a,b].

Catalysts	TOF[c] (10^{-3} s^{-1})	Glucose Conv. (%)	Selectivity (%)[d]								Diols Selectivity (%)[f]
			EG	PG	BDO	Sor	Ery	Gly	5-HMF	Others[e]	
Ru-W/SiO$_2$	163	100	33.8	29.2	24.3	6.4	1.7	4.5	–	0.1	87.3
Ru-W/AC	232	99.3	28.9	33.2	18.1	7.5	2.7	9.0	–	0.6	80.2
Ru-W/CNFs	850	99.9	21.1	18.4	5.2	36.8	3.8	14.7	–	–	44.7
Ru/WO$_3$	496	87.5	55.9	12.7	–	1.5	–	–	29.9	–	68.6

[a] Reaction conditions: 0.5 catalyst, 4 MPa H2, 478 K, 5 wt. % glucose aqueous solution, GHSV (H2) = 2500 cm3 g-1 h-1, TOS 10 h.

[b] The data were taken at 3rd hour of time on stream, calculated based on the mole percent.

[c] Evaluated on the basis of the rate of glucose conversion per surface Ru atom by using Ru dispersion measured from H2-O2 titration technique. TOF was calculated based on the reaction data taken at 3rd hour of time on stream.

[d] sor = sorbitol, ery = erythritol, gly = glycerol.

[e] others: gas products, tetritols, pentitols, and mannitol etc.

[f] Total selectivity of ethylene glycol (EG), 1, 2-propylene glycol (PG), and 1, 2-butanediol (BDO).

were needed. Meanwhile, glycerol easily undergoes further degradation under an acid environment [37]. Hence, the enhanced selectivity of sorbitol and glycerol indicated that the Ru metal sites on the Ru-W/CNFs catalyst surface effectively act as a hydrogenation function but W sites have quite low C—C bond cleavage and dehydration capability due to the negligible acid amount, according to the data of NH$_3$-TPD (Fig. 6). This conclusion was also confirmed by the specific activities in the form of glucose turnover frequencies (TOFs; i.e., numbers of glucose molecules converted per Ru adsorption site per s). The dispersion of Ru, i.e., the fraction of surface Ru atoms in the whole Ru atoms, was measured by a H$_2$-O$_2$ titration technique (Table 1). As shown in Table 2, the Ru-W/CNFs catalyst exhibited highest TOFs ($850*10^{-3}$ s^{-1}). However, this high hydrogenation activity is connected with a low selectivity because a lot of the hydrogenation by-product sorbitol was detected. For the Ru-W/SiO$_2$ catalyst, the TOF was the lowest due to the highest dispersion of Ru. However, the highest dispersed Ru provided the most hydrogenation active sites, those effectively converted the intermediates formed from abundant acid sites to diols, resulting in the highest diols selectivity. It is considered that as the supported Ru has very high hydrogenation activity, the different dispersion of Ru could not significantly influence the conversion of glucose, but it would significantly contribute to the formation of acid sites from partial reduction of the supported WO$_3$. As the synergetic effect, the abundant formed acid sites guarantee the C—C bond cleavage and dehydration capability, meanwhile, the highly dispersed Ru provide more active sites to effectively hydrogenate the intermediates to diols, resulting in high activity and high diols selectivity of the Ru-W/SiO$_2$ catalyst. On the other hand, more Ru sites would keep the acidity from partial reduced WO$_3$ via hydrogen spill-over effects during the reaction, contributing to the stability of glucose conversion over the Ru-W/SiO$_2$ catalyst. Therefore, it is believed that the balance between the hydrogenation sites and acid sites is very important in glucose hydrolysis.

For Ru/WO$_3$ catalyst, the lowest conversion (87.5%) can be ascribed to the lowest specific surface area, which exposed fewer active sites for glucose hydrogenolysis. The significant change in the product distribution–more retro aldol reaction followed by hydrogenation products (ethylene glycol) and more isomerization (5-HMF as a product of the dehydration reaction of fructose)–can be explained by the good balance of the rates of RAC, hydrogenation and dehydration reactions. On the one hand, the highest WO$_3$ loading would promote the RAC reaction followed by hydrogenation on Ru sites with high TOFs ($496*10^{-3}$ s^{-1}), results in the highest ethylene glycol selectivity (55.9%) in lower diols [38]. On the other hands, the highest WO$_3$ loading with weak acidity (NH$_3$-TPD in Fig. 6 and Table 1) also contribute to the high selectivity (29.9%) of 5-HMF, because the formation of 5-HMF could proceed directly by glucose isomerization followed by fructose dehydration on acid sites [2,39]. As shown in Table 1, the specific surface area of Ru/WO$_3$ catalyst was only 4.5 m^2/g, which

consequently suppress the dispersion of Ru species on WO$_3$ surface, leads to the lower hydrogen spill-over effect on the reduction of WO$_3$, resulting in weak acidity of this catalyst as shown in Fig. 6. However, the acidity of Ru/WO$_3$ catalyst is favorite to forming EG product, resulting in the highest EG selectivity of 55.9%.

The stability of the Ru-W/SiO$_2$ catalyst was further investigated, as presented in Fig. 7, where the conversion of glucose and the selectivity of EG, 1, 2-PG, and 1, 2-BDO are plotted as the function of time-on-stream. It is observed that Ru-W/SiO$_2$ exhibits excellent stability for 50 h-on-stream, with conversion of glucose being about 100% and selectivity to lower diols around 87%, due to the highly dispersed active species and strong metal-support interaction which prevent the sintering or leaching of supported active metal. In contrast, the continuous deactivation for Ru-W/CNFs catalyst implied the leaching of active metal particles during the reaction and in turn suppressing the activity of RAC and hydrogenation reaction.

3.3. Surface chemical states of active species in Ru-W/SiO$_2$ and Ru-WO$_3$ catalysts

Fig. 8a and c shows the *ex-situ* XPS spectra of the Ru-W/SiO$_2$ catalyst in the fresh state. The W 4f spectrum (Fig. 8c) displays two main peaks attributed to W 4f$_{5/2}$ and W 4f$_{7/2}$ transitions from W^{6+} at 38.3 eV and 36.1 eV, suggesting that all of W species on the surface of support was present as WO$_3$ phase. In addition, Ru 3d$_{3/2}$ and Ru 3d$_{5/2}$ signals were observed at 286.7 eV and 283.3 eV (Fig. 8a), which is assigned to Ru^{6+} species in RuO$_3$ [40].

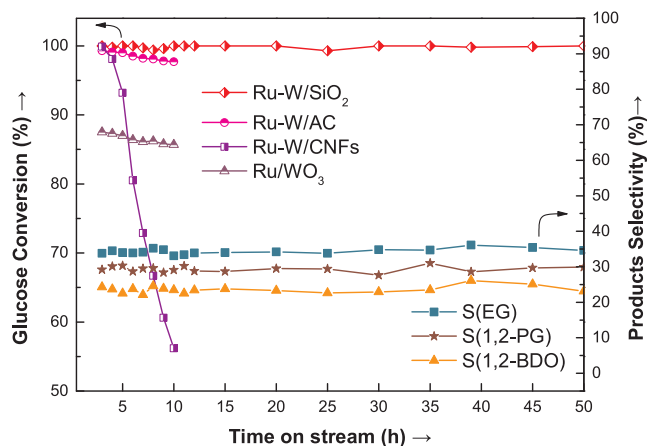In order to further investigate the surface structure of catalyst in the

Fig. 7. Long-term stability test of Ru-W/SiO$_2$ catalyst for glucose hydrogenation. Reaction conditions: 0.5 catalyst, 4 MPa H$_2$, 478 K, 5 wt. % glucose aqueous solution, GHSV = 2500 cm^3 g^{-1} h^{-1}, TOS 50 h.
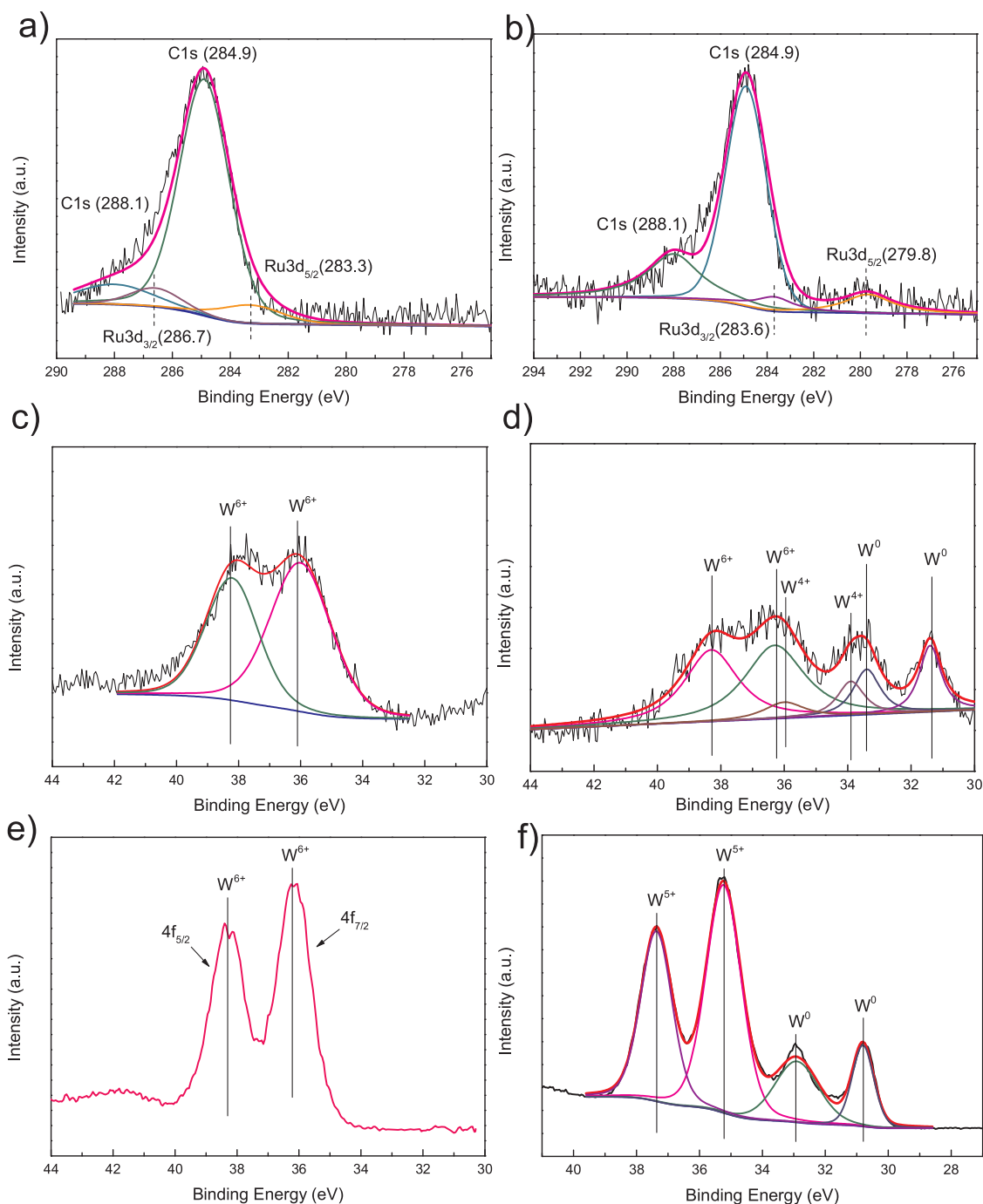
Fig. 8. a) *Ex-situ* XPS spectra in Ru 3d region from fresh Ru-W/SiO₂ catalyst; b) *in-situ* XPS spectra of Ru 3d core level recorded from Ru-W/SiO₂ catalyst after reduced; c, e) *Ex-situ* XPS spectra in W 4f region from fresh (c) Ru-W/SiO₂ and (e) Ru/WO₃ catalysts, respectively; d, f) *in-situ* XPS spectra of W 4f core level recorded from (d) Ru-W/SiO₂ and (f) Ru/WO₃ catalysts after reduced, respectively. The pre-reduced catalyst was reduced in-situ in H₂ at 648 K for 2 h.

real reaction conditions, *in-situ* XPS spectra of the supported Ru-W/SiO₂ catalyst was carried out to examine the evolution of chemical state of surface W and Ru species in the sample. Before the *in-situ* character-ization, the pre-reduced and passivated sample was reduced *in situ* at 648 K for 1 h using H₂. As shown in Fig. 8d, for the reduced Ru-W/SiO₂ catalyst, the W 4f XPS spectra consisted of multiple overlapping doublets at binding energies 31.3–38.3 eV. After deconvolution, the W $4f_{5/2}$ and W $4f_{7/2}$ spin orbit doublets at 38.3 eV and 36.3 eV are at-tributed to W^{6+} atoms, and doublet peaks around 35.9 eV and 33.9 eV are ascribed to W^{4+} atoms. Another two fitted peaks at binding en-ergies of 33.4 eV and 31.3 eV were characteristic of W° species [27]. As compared to the fresh catalyst, the presence of low valence W species in

Ru-W/SiO₂ catalyst arises from the reduction of WO₃ with pressured H₂ in the reduction process. The quantitative analysis result for the XPS spectra was listed in Table 1. For reduced Ru-W/SiO₂ catalyst, the predominant oxidation state for reduced W species was W^{4+} with a relative abundance of 16.1%, which is proposed to be advantageous to RAC reaction.

In-situ XPS related to Ru signals are displayed in Fig. 8b. The peak at 284.9 and 288.1 eV can be ascribed to the spectra of C 1 s of the stan-dard graphite carbon and adsorbed carbonates [41], which were pre-sumably picked up during exposed to the air or produced during the calcination and drying process. The peak at 279.8 eV in the Ru $3d_{5/2}$ region can be ascribed to the Ru° species [41,42], while Ru $3d_{3/2}$

spectrum was overlapped by C 1 s spectra at 283.6 eV. As compared to the *ex-situ* spectra of fresh Ru-W/SiO$_2$ catalyst (Fig. 8a), it can be found that almost all of Ru^{6+} were reduced to Ru° species during reduction process.

For Ru-W/SiO$_2$ catalyst, because the noble metal Ru is very easy to be reduced as illustrated by XPS and TPR results, the highest dispersion of Ru contributes to form more sites to activate hydrogen during the reduction step, and the activated hydrogen would reduce the supported WO$_3$ by spill-over effects to generate more surface W^{4+} species (as confirmed by *in-situ* XPS), contributing to forming more acid sites. However, the highly dispersed WO$_3$, induced by the largest surface area of silica support, strongly interacts with the silica support, which would influence the reducibility of the supported WO$_3$ as proved by TPR, resulting in a lot of unreduced WO$_3$ species, contributing to formation of suitable acidity for glucose conversion. Hence, it is proposed that the catalytic performance of Ru-W/SiO$_2$ catalyst was significantly improved due to the synergetic effect of abundant W^{4+} species and samll noble metal Ru° particles.

In addition, as shown in Table 2, it was found that the product distribution of Ru/WO$_3$ catalyst is distinct from the other catalysts. Among the lower diols, ethylene glycol became the main products. After 3 h reaction, ethylene glycol was obtained as high as 55.9% selectivity while 1, 2-BDO was absent in the products, although the total conversion of glucose was relatively lower (87.5%) than Ru-W/SiO$_2$. To understand the state of surface tungsten species on Ru/WO$_3$ catalyst, we also conduct the *ex-situ/in-situ* XPS spectra in W 4f region, as compared in Fig. 8e–f. In the case of fresh sample, the two intense peaks at 38.3 eV and 36.2 eV can be attributed to the surface W^{6+} species, which was similar to that of Ru-W/SiO$_2$. However, after reduction, the signals characteristic of W^{5+} and W° species appeared with intense peaks, while those of W^{6+} species disappeared. After deconvolution, the percentage of surface W^{5+} species was calculated as high as 82.0%. The formation of a large proportion of partially reduced WO$_x$ (W^{5+}) can be attributed to the reduction of Ru/WO$_3$ with pressured H$_2$ in the reduction process. As indicated by the above results, the Ru/WO$_3$ catalyst shows excellent selectivity to EG. Meanwhile, the W species in this catalyst are mainly present as W^{5+} species. This indicates that the W^{5+} species plays the vital role in the EG production. Hamdy et al. [43] found that the oxygen vacancies in the partially reduced W^{5+} species can absorb the oxygen of glucose which assists the rapid formation of C$_2$ intermediates (glycolaldehyde), which can further hydrogenated to EG over the metal sites. Fan et al. [36] also reported one-pot hydrogenolysis of cellulose to EG on WO$_3$-based catalysts, and found that the EG yield has a positive correlation with the surface W^{5+}/W^{6+} ratio of the spent catalyst. Hence, in the present work, it can be deduced that the formed W^{5+} species of Ru/WO$_3$ catalyst after reduced can act as active catalytic site for cleaving the C—C bond of the glucose molecule and further to C$_2$ intermediates (glycolaldehyde), which would promote the formation of EG.

Herein, glucose hydrogenolysis to lower diols is considered as a bifunctional reaction, involving the retro-aldol condensation reaction of glucose or fructose (the isomerization of glucose to fructose) to glycolaldehyde, glyceraldehydes, erythrose and dihydroxyacetone on WO$_x$ acid sites, as well as further hydrogenated to diols on Ru (0) metal sites. For Ru-W/SiO$_2$ catalysts, the highly dispersed Ru and WO$_3$ contributes to forming more surface W^{4+} species (as confirmed by *in-situ* XPS), which can form more acid sites for hydrolysis of glucose to C$_2$-C$_4$ intermediates by selectively cleaving C—C bond in glucose molecule. Additionally, the formed Ru° species act as hydrogenation sites for conversion of C$_2$-C$_4$ intermediates to lower diols. The highest glucose conversion and diols selectivity of Ru-W/SiO$_2$ can be ascribed to the high surface area with abundant reduced W^{4+} species and Ru° species, which would increase the amount of surface active sites for RAC and hydrogenation reaction. Meanwhile, Ru/WO$_3$ catalyst contributes to forming W^{5+} species after reduction, which can act as active catalytic site for cleaving the C—C bond of the glucose molecule and further to C$_2$

intermediates (glycolaldehyde), resulting in high selectivity of EG. In a word, the adequate acid sites and relatively high activity of hydrogenation are both important for the conversion of glucose to lower diols. However, too high TOFs were disadvantageous to produce lower diols, because excessive hydrogenation capacity will leads to the formation of more by-products such as sorbitol.

4. Conclusions

Selective hydrogenation of glucose into lower diols over various Ru-W supported catalysts was investigated in a continuous-flow fixed-bed reactor system. Based on various characterizations, we have discovered that the dispersion of the tungsten and ruthenium species, as well as the number of surface acid groups with moderate acid strength, are crucial for tuning the balance of C—C bond breaking activity and hydrogenation capacity. In addition, the strong metal-support interaction can effectively inhibited the leaching of active WO$_x$ species on the support, which gave a stable catalytic performance on abundant W^{4+} surface species. Among all the catalysts, the highly dispersed Ru-W/SiO$_2$ catalyst shows a high resistance for catalyst deactivation (TOS 50 h) with highest glucose conversion (100%) and diols selectivity (87.3%) due to the synergistic effects of the highly dispersed Ru° species and abundant acid sites on W^{4+} species. On the other hand, Ru/WO$_3$ catalyst contributes to forming W^{5+} species, which is advantageous to forming EG products.

Conflict of interest

The authors declare no competing financial interest.

Acknowledgment

References

[1] X. Zhang, L.J. Durndell, M.A. Isaacs, C.M.A. Parlett, A.F. Lee, ACS Catal. 6 (2016) 7409–7417.
[2] J. Song, H. Fan, J. Ma, B.X. Han, Green Chem. 15 (2013) 2619–2635.
[3] M. Yabushita, H. Kobayashi, A. Fukuoka, Appl. Catal. B 145 (2014) 1–9.
[4] C. Liu, C. Zhang, S. Sun, K. Liu, S. Hao, J. Xu, Y. Zhu, Y.W. Li, ACS Catal. 5 (2015) 4612–4623.
[5] Q. Yuan, A.X. Yin, C. Luo, L.D. Sun, Y.W. Zhang, W.T. Duan, H.C. Liu, C.H. Yan, J. Am. Chem. Soc. 130 (2008) 3465–3472.
[6] J. Pang, M. Zheng, X. Li, Y. Jiang, Y. Zhao, A. Wang, J. Wang, X. Wang, T. Zhang, Appl. Catal. B 239 (2018) 300–308.
[7] L.S. Ribeiro, J.J. Delgado, J.J.M. Órfão, M.F.R. Pereira, Appl. Catal. B 217 (2017) 265–274.
[8] P.A. Lazaridis, S.A. Karakoulia, C. Teodorescu, N. Apostol, D. Macovei, A. Panteli, A. Delimitis, S.M. Coman, V.I. Parvulescu, K.S. Triantafyllidis, Appl. Catal. B 214 (2017) 1–14.
[9] J.C. Serrano-Ruiz, D.J. Braden, R.M. West, J.A. Dumesic, Appl. Catal. B 100 (2010) 184–189.
[10] M.S. Holm, S. Saravanamurugan, E. Taarning, Science 328 (2010) 602–605.
[11] F. Chambon, F. Rataboul, C. Pinel, A. Cabiac, E. Guillon, N. Essayem, Appl. Catal. B 105 (2011) 171–181.
[12] F. Jin, J. Yun, G. Li, A. Kishita, K. Tohji, H. Enomoto, Green Chem. 10 (2008) 612–615.
[13] J.B. Binder, R.T. Raines, J. Am. Chem. Soc. 131 (2009) 1979–1985.
[14] J. Wang, J. Ren, X. Liu, J. Xi, Q. Xia, Y. Zu, G. Lu, Y. Wang, Green Chem. 14 (2012) 2506–2512.
[15] J. Guo, S. Zhu, Y. Cen, Z. Qin, J. Wang, W. Fan, Appl. Catal. B 200 (2017) 611–619.
[16] K. Yan, Y. Yang, J. Chai, Y. Lu, Appl. Catal. B 179 (2015) 292–304.
[17] M. Zheng, J. Pang, R. Sun, A. Wang, T. Zhang, ACS Catal. 7 (2017) 1939–1954.
[18] A. Aho, S. Roggan, O.A. Simakova, T. Salmi, D.Y. Murzin, Catal. Today 241 (2015) 195–199.
[19] A. Fukuoka, P.L. Dhepe, Angew. Chem. Int. Ed. 45 (2006) 5161–5163.
[20] C. Luo, S. Wang, H. Liu, Angew. Chem. Int. Ed. 46 (2007) 7636–7639.
[21] Y. Liu, C. Luo, H. Liu, Angew. Chem. Int. Ed. 51 (2012) 3249–3253.

[22] J. Na, T. Zhang, M. Zheng, A. Wang, H. Wang, X. Wang, J.G. Chen, Angew. Chem. Int. Ed. 47 (2008) 8510–8513.

[23] X. Wang, L. Meng, F. Wu, Y. Jiang, L. Wang, X. Mu, Green Chem. 14 (2012) 758–765.

[24] K.C. Taylor, J. Catal. 38 (1975) 299–306.

[25] C. Yuan, N. Yao, X. Wang, J. Wang, D. Lv, X. Li, Chem. Eng. J. 260 (2015) 1–10.

[26] Y. Liu, J.F. Chen, Y. Zhang, RSC Adv. 5 (2015) 29002–29007.

[27] S.J. You, I.G. Baek, E.D. Park, Appl. Catal. A 466 (2013) 161–168.

[28] M. Signoretto, E. Ghedini, F. Menegazzo, G. Cerrato, V. Crocellà, C.L. Bianchi, Microporous Mesoporous Mater. 165 (2013) 134–141.

[29] M.A. Álvarez-Montero, L.M. Gómez-Sainero, A. Mayoral, I. Diaz, R.T. Baker, J.J. Rodríguez, J. Catal. 279 (2011) 389–396.

[30] B. Li, S. Kado, Y. Mukaiminato, T. Miyazawa, T. Miyao, S. Naito, K. Okumura, K. Kunimori, K. Tomishige, J. Catal. 245 (2007) 144.

[31] E.I. Ross-Medgaarden, I.E. Wachs, J. Phys. Chem. C 111 (2007) 15089–15099.

[32] G. Lu, X. Li, Z. Qu, Y. Wang, G. Chen, Appl. Surf. Sci. 255 (2008) 3117–3120.

[33] C.V. Ramana, S. Utsunomiya, R.C. Ewing, C.M. Julien, U. Becker, J. Phys. Chem. B 110 (2006) 10430.

[34] I.M. Szilágyi, B. Fórizs, O. Rosseler, A. Szegedi, P. Németh, P. Király, G. Tárkányi, B. Vajna, K. Varga-Josepovits, K. László, A.L. Tóth, P. Baranyai, M. Leskelä, J. Catal. 294 (2012) 119–127.

[35] Y. Liu, D. Li, T. Wang, Y. Liu, T. Xu, Y. Zhang, ACS Catal. 6 (2016) 5366–5370.

[36] J. Chai, S. Zhu, Y. Cen, J. Guo, J. Wang, W. Fan, RSC Adv. 7 (2017) 8567–8574.

[37] D. Sun, Y. Yamada, S. Sato, Appl. Catal. A 487 (2014) 234–241.

[38] M. Lucas, K. Fabicovicova, P. Claus, ChemCatChem 10 (2018) 612–618.

[39] Q. Hou, M. Zhen, L. Liu, Y. Chen, F. Huang, S. Zhang, W. Li, M. Ju, Appl. Catal. B 224 (2018) 183–193.

[40] S. Kim, K. Qadir, S. Jin, A.S. Reddy, B. Seo, B.S. Mun, S.H. Joo, J.Y. Park, Catal. Today 185 (2012) 131–137.

[41] X. Lin, K. Yang, R. Si, X. Chen, W. Dai, X. Fu, Appl. Catal. B 147 (2014) 585–591.

[42] E. Lee, A. Murthy, A. Manthiram, J. Electroanal. Chem. 659 (2011) 168–175.

[43] M.S. Hamdy, M.A. Eissa, S.M.A.S. Keshk, Green Chem. 19 (2017) 5144–5151.